Check for updates

Crystalline engineering of FAPbI₃ *via* pyrrolidinium ionic liquid for stable perovskite solar cells with 21.72% efficiency

Anjan Kumar, [ID] [a] Mandeep Kaur, [bc] M. Atif, [d] Jatinder Kaur, [e] Ramneet Kaur, [fg] Mohammed A. El-Meligy, [hi] Parminder Singh[j] and Merwa Alhadrawi [ID] *[kl]

Improving the crystallinity of formamidinium triiodide (FAPbI₃) perovskite layer is one of the most effective approaches to increase the photovoltaic performance and stability of FAPbI₃-based solar cells (FSCs). In the current study, FAPbI₃ layers were fabricated through a sequential deposition method. The morphology and crystalline properties of the FAPbI₃ layers were modified by controlling the lead iodide (PbI₂) precursor by adding pyrrolidinium (Pyr) material into the PbI₂ layer and modulating the FAPbI₃ crystallization. The Pyr contributed to obtain (001)-preferred FAPbI₃ orientation with no yellow photo-inactive phase. Subsequently, it reduced the unreacted PbI₂ phase in the perovskite layer and suppressed the defect density, resulting in extended carrier lifetimes and improved ambient air and illumination stabilities. The Pyr-mediated FSCs recorded a champion efficiency of 21.72%, which is higher than that of control FSCs with a maximum efficiency of 19.08%. The developed Pyr-mediated method offers a practical and effective approach to fabricate stable and efficient FSCs.

1. Introduction

Given the depletion of fossil fuels, steady rise in environmental pollution and energy consumption worldwide, there is a growing need for research on renewable and sustainable energy sources.[1–3] Using renewable energy is one of the most encouraging ways to meet the rising demands of electricity for future generations without negatively impacting the global environment.[4] Tidal, hydroelectric, geothermal, and solar energy are a few examples of these renewable energy sources. Light energy can be converted into electricity using solar cell technology, which is a sustainable and environmentally benign energy source.

Since the introduction of metal halide perovskite solar cells (PSCs) in 2009, their power conversion efficiency (PCE) has displayed substantial progress, rising from 3.8% to 26.1%.[5–8] These advancements in conversion efficiencies can be attributed to the effective passivation of different defects present in perovskite thin films, as well as the enhanced suppression of non-radiative recombination processes.[9–13] The formamidinium-based perovskite (FAPbI₃), among the various organic–inorganic hybrid perovskites available, has garnered significant attention due to the numerous advantages it offers. These include a larger and thermally stable organic formamidinium (FA) cation that can substitute for the less stable methylammonium (MA) cation, a narrow energy bandgap that facilitates near-infrared absorption, and a higher decomposition temperature. FAPbI₃ is considered the most capable material for high-efficiency solar cells due to its tunable bandgap (ranging from 1.5 to 1.4 eV), low exciton binding energy (less than 50 mV), high absorption coefficient in the range of 10^4 to 10^5 cm^{-1}, and long charge carrier diffusion length (ranging from 0.1 to 1.0 μm).[14–16]

Perovskite films mainly consist of four types of defects: three-dimensional lead clusters, point defects, intrinsic impurities,

[a]Department of Electronics and Communication Engineering, GLA University, Mathura-281406, India

[b]Department of Chemistry, School of Sciences, Jain (Deemed-to-be) University, Bengaluru, Karnataka-560069, India

[c]Department of Sciences, Vivekananda Global University, Jaipur, Rajasthan-303012, India

[d]Department of Physics and Astronomy, College of Science, King Saud University, P O Box 2455, Riyadh 11451, Saudi Arabia

[e]Department of Electronics and Communication Engineering, Division of Research & Innovation, Chandigarh Engineering College, Chandigarh Group of Colleges Jhanjeri, Mohali-140307, Punjab, India

[f]Department of Electronics and Communication and Electrical Engineering, Shobhit University, Gangoh, Uttar Pradesh, 247341, India

[g]Department of Electrical and Electronics Engineering, Arka Jain University, Jamshedpur, Jharkhand-831001, India

[h]Applied Science Research Center, Applied Science Private University, Amman, Jordan

[i]Jadara University Research Center, Jadara University, PO Box 733, Irbid, Jordan

[j]Centre for Research Impact & Outcome, Chitkara University Institute of Engineering and Technology, Chitkara University, Rajpura, 140401, Punjab, India

[k]Department of Refrigeration and Air Conditioning Techniques, College of Technical Engineering, The Islamic University, Najaf, Iraq. E-mail: Merwa.Alhadrawi7211@outlook.com

[l]Department of Refrigeration and Air Conditioning Techniques, College of Technical Engineering, The Islamic University of Al Diwaniyah, Al Diwaniyah, Iraq

and grain boundaries. These defects may negatively affect generated carrier movement and aggregation, leading to non-radiative recombination. In addition, they may serve as pathways for ion migration, thereby accelerating the deterioration of perovskite materials.[17,18] Additionally, poor surface and grain boundaries might act as direct pathways for the entry of air and moisture.[19] In order to tackle these challenges, defect passivation has emerged as a highly effective approach for addressing the long-term stability of perovskite materials from within.

Researchers worldwide are actively addressing the challenges associated with perovskite devices, focusing on various factors such as the development of superior absorber materials, high-quality films, efficient charge injection and extraction, and durable constituent materials. To improve the efficiency and stability of perovskite devices, there has been significant interest in utilizing ionic liquids. These liquids exhibit exceptional versatility due to their distinct and intriguing properties. Ionic liquids have been extensively studied for several decades and have found applications in various fields, including synthesis, catalysts, energy, and medicine.[20,21]

Impressive progress has been made in the exploration of ionic liquids (ILs), a family of molten salts having a melting temperature below 100 °C, for potential use in PSCs. Different organic cations (such as triazolium, imidazolium, piperidinium, ammonium, pyrrolidinium, pyridinium, and phosphonium) and organic or inorganic anions (such as phosphate, halide, sulfonic acid, tetrafluoroborate, hexafluorophosphate, carboxylic acid, and imide) are typically found in ILs. In general, ILs exhibit a wide range of special qualities, including strong conductivity, solvate capability, low toxicity, wide electrochemical window, and wide liquid range. Notably, ILs have been extensively studied in the realm of PSCs and have demonstrated various functionalities in the development of efficient and durable PSC devices.[22,23]

Achieving a smooth and homogeneous morphology in perovskite films is crucial for enhancing the performance and stability of the devices.[24] Shahiduzzaman *et al.*[25] employed a facile spin coating technique and added 1 wt% of the ionic liquid 1-hexyl-3-methylimidazolium chloride (HMImCl) to a 25 wt% solution of MAPbI$_3$ in DMF. This approach resulted in a uniform MAPbI$_3$ film without pinholes. Wan and co-worker used[26] 1-ethylpyridinium chloride (1-EC) ionic liquid in a one-step approach on a PEDOT:PSS substrate to study an inverted perovskite solar cell. Experimental results showed remarkable surface coverage, and these ionic liquids were able to produce a pinhole-free MAPbI$_3$ film. The non-passivated sample had photovoltaic PCEs that were less than half of those of optimized devices, which had an optimal concentration of 1 weight percent IL. Seo *et al.*[27] fabricated a compact perovskite absorber layer on an FTO substrate covered with SnO$_2$ by using the ionic liquid methylammonium formate (MAFa) in another investigation. This approach aimed to improve the film quality. In this study, the advantages of incorporating Pyr-ionic liquid into the PbI$_2$ layer of FPSCs was investigated to enhance their performance and stability. By fabricating solar cells with varying concentrations of Pyr and conducting a range of analyses, it was found that the optimal amount of Pyr significantly enhanced

PCEs, charge carrier dynamics, and crystal growth within the perovskite film. The inclusion of Pyr also led to reduced recombination losses, improved interfacial carrier transfer dynamics, and lower recombination rates, all contributing to higher device efficiency. Additionally, Pyr-IL modification enhanced the stability of PSCs under ambient air and continuous illumination conditions. Overall, these findings highlight the positive impact of Pyr in advancing the performance and stability of FSC, offering promising prospects for future renewable energy technologies.

2. Materials and methods

2.1. Solar cell preparation

A 66 mM SnCl$_2 \cdot$2H$_2$O solution was prepared in ethanol (99.8%, Merck) and 50 μL of it was spin-coated over the FTO at 3350 rpm for 30 s. Then, the prepared layers were annealed in air at 195 °C for 55 min. Here, to fabricate the FAPbI$_3$ light-harvesting layer, sequential deposition method was employed. First, lead iodide (PbI$_2$, 99.99%, SunLab) was dissolved into dimethyl sulfoxide (99.9%, Merck) and dimethylformamide (99.8%, Merck) mixed solvent (1 : 4 v/v) to obtain a 1.4 M PbI$_2$ precursor. The PbI$_2$ solution was stirred at 80 °C for 30 min, and then 50 μL of it was spin coated over the SnO$_2 \cdot$ETL at 1600 rpm for 15 s and 4100 rpm for 45 s. The primitive PbI$_2$ layers were annealed at 90 °C for 45 s. To prepare the pyrrolidinium + PbI$_2$ solutions, different amounts of pyrrolidinium (Pyr, 99.7%, Sigma-Aldrich) material were poured into the PbI$_2$ solution and stirred at 50 °C for 30 min. Deposition of Pyr–PbI$_2$ solution is the same as the pure PbI$_2$ solution. Second, FAI/MACl/MABr precursor was prepared by dissolving 110 mg formamidinium iodide (FAI, 99.9%, Sigma-Aldrich), 11 mg methylammonium bromide (MABr, 99.9%, Sigma-Aldrich), and 11 mg methylammonium chloride (MACl, 99.9%, Sigma-Aldrich) in 1 mL isopropyl alcohol. 50 μL of FAI/MACl/MABr precursor was spin coated over the PbI$_2$ or Pyr–PbI$_2$ layer at a speed of 2000 rpm for 20 s, followed by annealing at 145 °C for 13 min. Thereafter, standard 2,2′,7,7′-tetrakis[*N*,*N*-di(4-methoxyphenyl)amino]-9,9′-spirobifluorene (Spiro-OMeTAD, 99%, Sigma-Aldrich) solution was prepared as reported in literature, and 60 μL of it was deposited on the FAPbI$_3$ light-harvesting layer at 4000 rpm for 30 s. At the end, 100 nm gold electrodes were evaporated over the hole transport layer (HTL). The proposed layered device configuration is depicted in Fig. 1. It should be noted that all fabrication steps were conducted in ambient air with a relative humidity of 25%.

2.2. Measurements

An electrochemical potentiostat (Zahner Zennium) was used to measure the electrochemical impedance spectra (EIS) of samples. The morphology of photoactive layers was investigated by recording top-view FESEM images using a TESCAN FESEM instrument (Mira3). An X-ray diffractometer (XRD, STAD IP) was employed to record XRD patterns of films. A UV-VIS Thermo Biomate5 spectrophotometer was used to measure the absorbance spectra of perovskite films. Photoluminescence (PL)
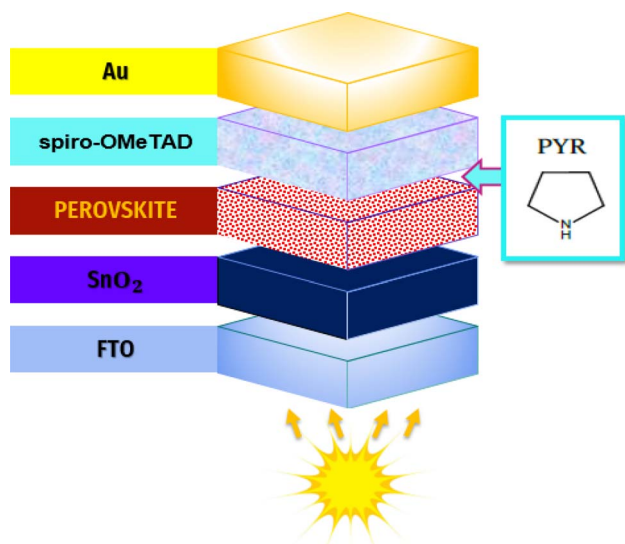
curves of photoactive layers were measured using a PL Varian device. *J–V* curves of PSCs under simulated sunlight (calibrated with a silicon solar cell) or hole-only devices under dark conditions with an active area of 2 mm × 4 mm were recorded using a Keithley 2400 source. AFM images of perovskite layers were obtained using a BIRISK AFM instrument.

3. Results and discussion

To investigate the advantages of incorporating Pyr material into the PbI_2 layer of FSCs, solar cell devices were fabricated with different percentages of Pyr added into the PbI_2 layer using the FTO/ETL/perovskite/HTL/Au device structure. The performances of these FSCs were evaluated by measuring the *J–V* curves under AM 1.5G illumination conditions. The results, as summarized in Table 1, indicate that the introduction of Pyr led to improved power PCE in the devices. The enhancement in PCE was directly proportional to the percentage of Pyr used. Notably, the highest PCE of 21.72% was achieved when the device was fabricated with 1.75% Pyr. This suggests that 1.75% Pyr added into the PbI_2 layer is the optimal amount for achieving the best PCE. These findings emphasize the positive impact of Pyr in

FSCs, attributed to factors such as enhanced charge carrier transport, reduced recombination losses, and improved device stability. The presence of Pyr IL contributes to the improved device performance, leading to higher PCE.

Fig. 2a illustrates the *J–V* characteristics of the optimized FSCs using control and Pyr-mediated perovskite layers. These measurements were performed under AM 1.5G illumination, comparing samples with and without the presence of IL. In the absence of IL, the device exhibited a J_{sc} of 24.37 mA cm^{-2}, V_{oc} of 1.095 V, FF of 71.57%, and PCE of 19.08%. In contrast, with IL, the device showed a J_{sc} of 24.47 mA cm^{-2}, V_{oc} of 1.125 V, FF of 78.8%, and PCE of 21.72%. The inclusion of IL in the films resulted in an enhanced PCE compared to the control (without IL). To investigate the hysteresis behavior of FSCs, the *J–V* responses of a typical FSC as control and Pyr-mediated group with different voltage-sweep directions were measured (Fig. 2b). To measure the hysteresis index (HI) of samples, the equation

$$HI = \left(\frac{PCE_{reverse} - PCE_{forward}}{PCE_{reverse}} \right) \times 100\%$$ was used. Values of

11.14% and 3.44% were obtained for the control and Pyr-mediated FSCs, respectively. To gain further insight into the effects of the addition of Pyr concentration on the crystalline qualities of films and the optoelectronic properties of the FSCs, the optoelectronic attributes and charge transfer/recombination kinetics of the films were investigated using steady-state photoluminescence (PL), as shown in Fig. 2c. The Pyr-mediated perovskite layers have higher PL peak intensity compared to the pure perovskite film. Increasing the concentration of Pyr from 0.5 to 1.75 wt% initially boosted the PL peak intensity, but it then decreased in the case of 2.25 wt%. The highest intensity was achieved at 1.75 wt%. As a result, the passivation impact of Pyr on defects might be responsible for the varying intensities of the PL peaks. The defect state density in the perovskite film and at the interface between the electron transport layer (ETL) and the perovskite film reaches its minimum level when the concentration is 1.75%. It is important to remember that IL concentrations shouldn't be excessively high, as it may have an impact on the film's solubility and cause an uneven coating, which would then have an impact on the perovskite's future growth and crystallization.

To examine how Pyr affects the transfer dynamics of carriers at the interface in FSCs, electrochemical impedance spectroscopy (EIS) measurements were performed in the absence of

Table 1 Photovoltaic parameters of control and treated FSCs

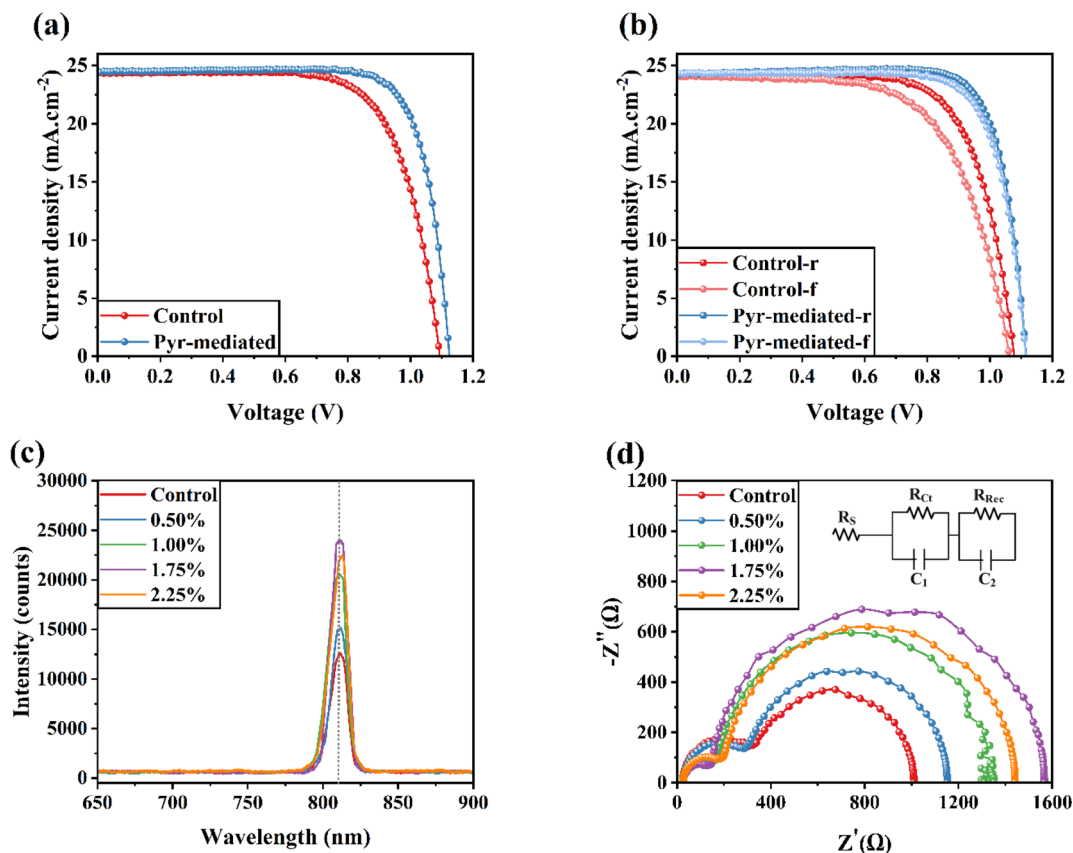| Device		V_{OC} (V)	J_{SC} (mA cm^{-2})	FF (%)	PCE (%)
Control	Average	1.077 ± 0.013	24.18 ± 0.13	70.84 ± 0.52	18.42 ± 0.37
	Best	1.095	24.37	71.57	19.08
0.50%	Average	1.090 ± 0.011	24.20 ± 0.17	71.91 ± 0.91	18.98 ± 0.51
	Best	1.105	24.41	73.05	19.70
1.00%	Average	1.100 ± 0.012	24.31 ± 0.14	75.40 ± 0.49	20.17 ± 0.35
	Best	1.115	24.46	76.13	20.76
1.75%	Average	1.115 ± 0.008	24.30 ± 0.13	78.33 ± 1.05	21.22 ± 0.31
	Best	1.125	24.47	78.87	21.72
2.25%	Average	1.107 ± 0.010	24.31 ± 0.17	76.38 ± 0.95	20.56 ± 0.39
	Best	1.115	24.54	76.93	21.05

Fig. 2 (a) $J-V$ curves of the optimized FSCs based on control and Pyr-mediated perovskite layers. (b) $J-V$ curves of typical FSCs in reverse and forward directions in each group. (c) PL spectra of different perovskite layers fabricated on glass substrates. (d) EIS responses of different FSCs measured at open-circuit voltage in dark conditions. Inset of (d) shows equivalent electrical circuit to fit Nyquist plots.

light at the open-circuit voltage. Fig. 2d displays the Nyquist plots for different FSCs. The results demonstrate that incorporating Pyr into the PbI_2 layer enhances the charge carrier dynamics within the FSCs, leading to improved photovoltaic parameters (refer to Table 1). In particular, the photovoltaic solar cells containing 1.75% Pyr demonstrate a noticeably high charge recombination resistance (R_{rec}) value of 1418.2 Ω. In contrast, the control devices and the FSCs with 2.25% Pyr show reduced R_{rec} values of 684.2 and 1241.4 Ω, respectively. This indicates that the electron–hole recombination rate at the interfaces can be mitigated with the optimal Pyr concentration.[28] The impedance graph further suggests that the integration of Pyr improves the internal electrical properties of the FSCs, potentially resulting in lower charge transfer resistance and higher charge collection efficiency. These findings highlight the positive influence of Pyr on the interfacial carrier transfer dynamics in FSCs. Overall, the recorded R_{rec} values for the control, 0.50%-, 1.00%-, 1.25%-, 1.75%-, and 2.25%-Pyr mediated perovskite layers are 684.2, 854.3, 1187.3, 1418.2, and 1241.4 Ω. In addition, the recorded R_{ct} values for the control, 0.50%-, 1.00%-, 1.25%-, 1.75%-, and 2.25%-Pyr mediated perovskite layers are 301.41, 271.32, 152.93, 122.81, 174.36 Ω.

Our work aims to evaluate the influence of Pyr on the crystallization process of perovskite films, given the important role that perovskite morphology plays in the performance of FSCs;

this was evaluated using atomic force microscopy (AFM) and scanning electron microscopy (SEM). In comparison to the control, the SEM images of the Pyr-based perovskite films showed better coverage and bigger grain sizes (Fig. 3). Additionally, the SEM study shown in Fig. 3d showed that the perovskite layers based on 2.25% Pyr showed tiny voids and pinholes close to the grain boundaries. The perovskite layer based on 1.75% Pyr (Fig. 3c), on the other hand, showed full coverage and noticeably bigger grain sizes. Based on these data along with XRD (Fig. 5b, will be discussed later) and PL (Fig. 2c) observations, it can be concluded that the presence of Pyr increases the crystallinity of the perovskite layers. To support the claim of larger grain size in Pyr-mediated films, the statistical grain size distributions of the perovskite layers were measured and are depicted in Fig. 3e. As seen in Fig. 3e, the average perovskite grain size of the control layer is 769.8 nm, while that of the 1.75%-Pyr mediated perovskite layer increases to 1452.2 nm.

The AFM analysis provided additional evidence to support the aforementioned observation (Fig. 4a and b). The root mean square (RMS) roughness of the perovskite films with and without the inclusion of the Pyr IL were measured to be 24.19 nm and 36.13 nm, respectively. These results confirm that the addition of the Pyr IL in the spin-coating process leads to the formation of a smooth and uniform perovskite film. This
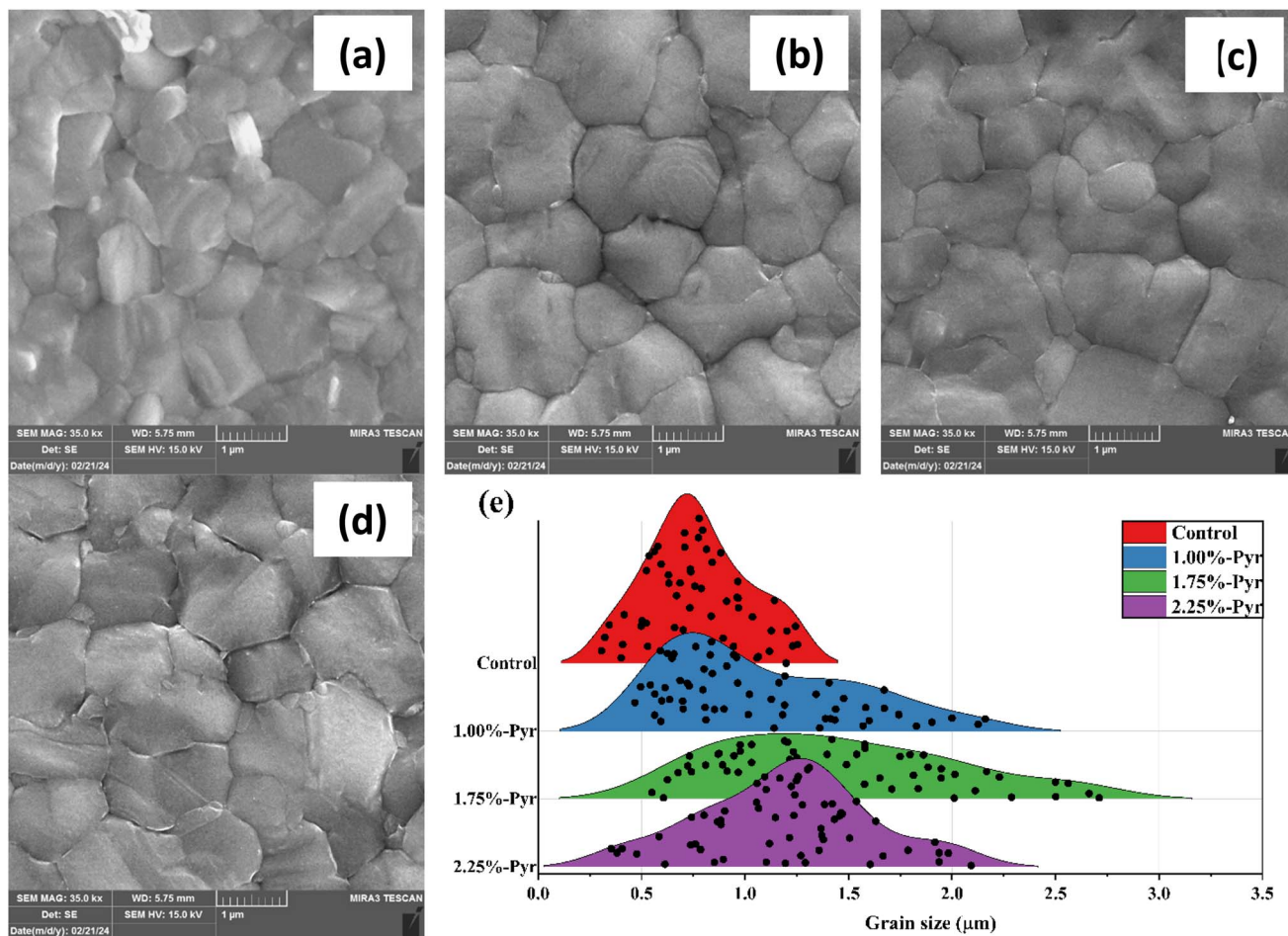

Fig. 3 FESEM images of (a) control, (b) 1.00%-, (c) 1.75%-, and (d) 2.25%-Pyr based perovskite layers. (e) Grain size distributions of different perovskite layers.

evidence suggests that the incorporation of an IL in the spin-coating of perovskite solution promotes enhanced surface smoothness and uniformity in the resulting perovskite films, as indicated by the significant decrease in RMS roughness compared to films without IL.

Fig. 5a displays the UV-Vis spectra of $FAPbI_3$ films, both with and without the presence of ionic liquids (IL). When comparing the UV-Vis absorption spectra of the Pyr-mediated perovskite film to that of the control, it is evident that they exhibit minimal differences. Expectations were met by the lack of appreciable differences in the UV-Vis spectra between the Pyr-mediated perovskite layer and the control. This is due to the Pyr cations' large size, which keeps them from fitting into the formamidinium lead triiodide lattice.

The produced perovskite layers' X-ray diffraction (XRD) patterns were examined, comparing samples with and without
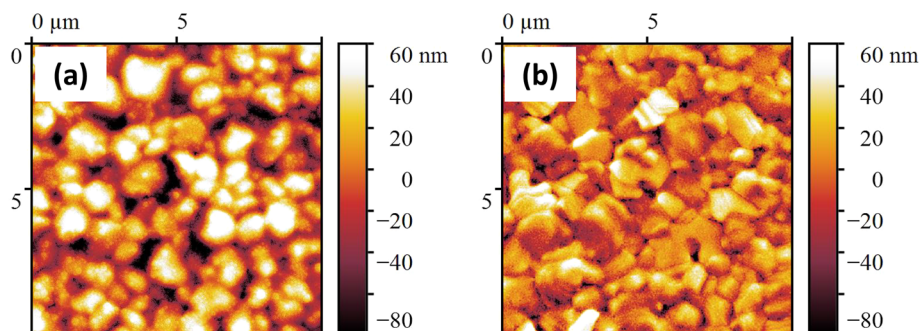

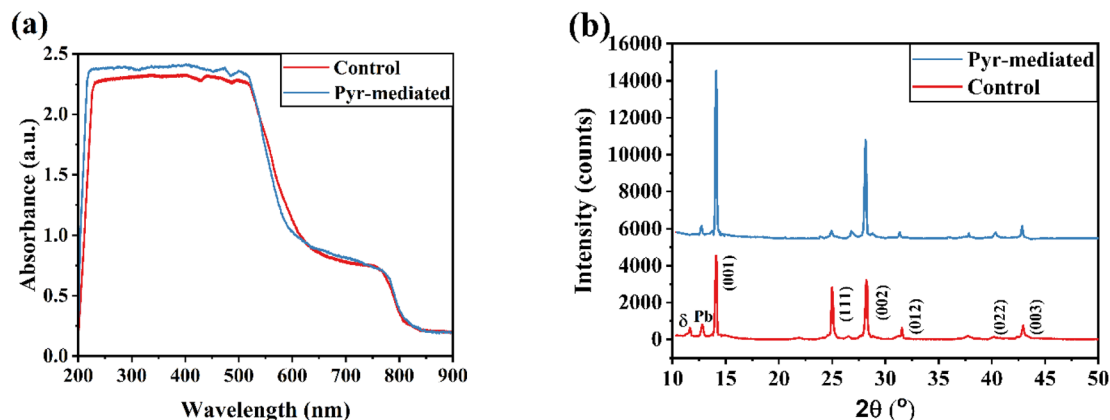Fig. 4 AFM images of (a) control and (b) Pyr-mediated perovskite layers.

Fig. 5 (a) Absorbance spectra and (b) XRD patterns of control and Pyr-mediated perovskite layers.

the inclusion of an IL (Fig. 5b). Both samples exhibited the same crystal structures, as evidenced by the presence of peaks at specific angles (2θ). The peaks observed at $2\theta = 14.09°$, $24.99°$, $28.21°$, $31.54°$, $40.49°$, and $42.96°$ corresponded to the crystal planes (001), (111), (002), (012), (022), and (003), respectively.[29,30] This demonstrates that FAPbI$_3$ perovskite has formed. The (001) peak's intensity increased after the IL was added to the perovskite, suggesting better crystal formation. Furthermore, the addition of Pyr material to the PbI$_2$ component resulted in a decrease in the primary peak's full width at half maximum (FWHM) at $14.09°$, from 0.177 to 0.147, without affecting its position. This decrease implies that the perovskite structure contains a higher degree of molecular organization. As a result, Pyr helps the FAPbI$_3$ film to have improved grain orientation and preferential growth along the (001) direction. During the annealing of perovskite films, the formation of a cubic PbI$_2$ structure can occur, leading to a detectable signal at $12.79°$ in the XRD pattern.[31] This signal serves as an indication of the presence of residual PbI$_2$ in the film. However, when the perovskite film is treated with Pyr, the intensity of the PbI$_2$ peak is reduced compared to that of the control cell. This reduction

implies a decrease in the quantity of remaining PbI$_2$ in the modified perovskite film.

There are two main reasons for the demand for bigger perovskite crystal sizes. First of all, because grain boundaries might serve as locations for charge recombination, it is preferable to minimize their existence. Second, larger crystal sizes may lessen the number of grain boundaries per volume, which would lessen the negative consequences of charge recombination. This improvement in crystal size can enhance both the open-circuit voltage (V_{oc}) and fill factor (FF) of a solar cell.[32,33] Larger perovskite crystals facilitate the movement of photoinduced charges over longer distances during charge transfer, leading to improved device performance.[34,35]

The relationship between the V_{oc} and light intensity was analyzed to determine the ideality factor (n), which is associated with trap-assisted recombination. The graph in Fig. 6 shows that the Pyr-mediated FSCs have a lower ideality factor ($n = 1.46$) compared to the control device ($n = 2.63$). This indicates a reduction in trap-assisted recombination in the Pyr-mediated FSCs.[36,37] The improved charge carrier dynamics within these FSCs are likely responsible for this decrease in the ideality
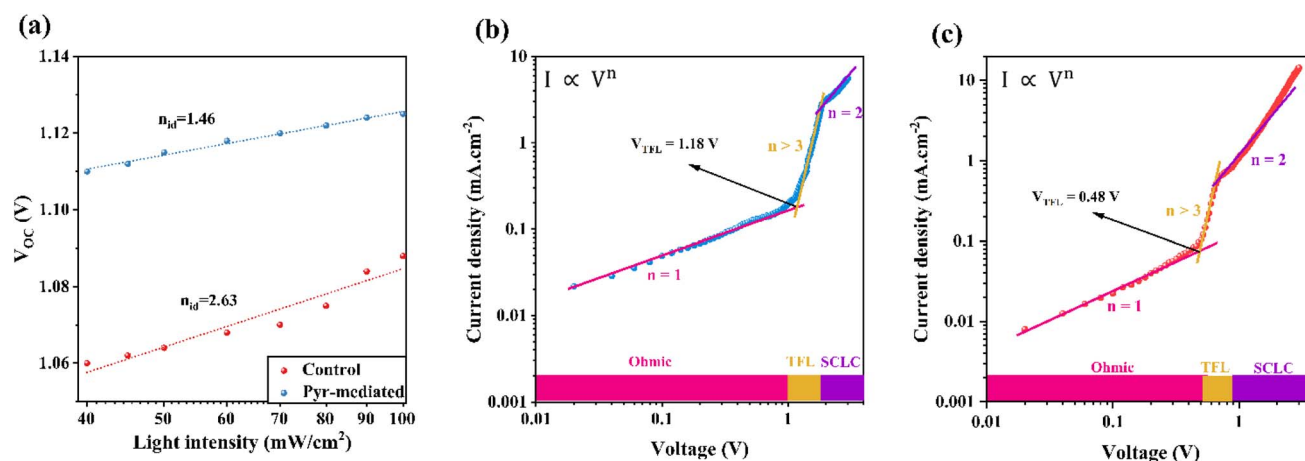

Fig. 6 (a) Voltage *versus* light intensity plot of control and Pyr-mediated PSCs. Dark SCLC curves for hole-only devices based on the (b) control and (c) Pyr-mediated perovskite films.
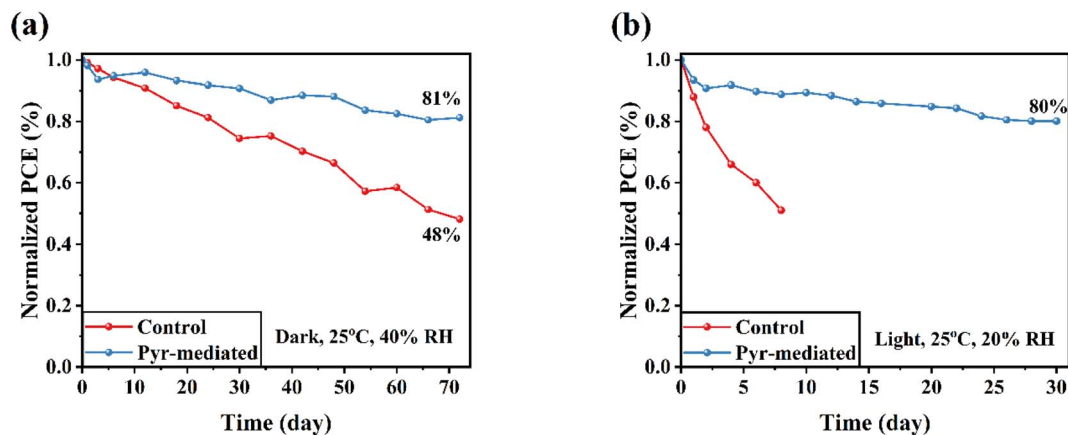
Fig. 7 Stability tests of unsealed control and Pyr–mediated FPSCs (a) in humid ambient air in dark condition and (b) in ambient air under simulated light irradiance.

factor. The lower n value suggests that the Pyr-mediated FSCs experience lower recombination rates, potentially leading to higher efficiencies in converting light into electricity.

To quantitatively characterize the defect properties of perovskite layers, space-charge limited current (SCLC) measurements were conducted on hole-only devices with a structure of FTO/PEDOT:PSS/bare or Pyr-mediated FAPbI$_3$/Spiro-OMeTAD/Au (Fig. 6b and c). As seen in Fig. 6b and c, the current enhances linearly with the voltage (ohmic region) up to a critical point, after which the current rises faster due to trap-state filling by the injected carriers. Then, by further increasing the voltage, the trap state is fully filled and a SCLC regime is created, where the current reveals a quadratic voltage dependence. The critical point's voltage is defined as the trap-filled limit voltage (V_{TFL}), which, as reported in ref. 38 and 39, is directly related to trap density. The electron trap densities of the control and Pyr-mediated samples were calculated to be 12.75×10^{15} and 5.19×10^{15} cm^{-3}, respectively. This demonstrates that the defects of the Pyr-mediated perovskite layer have been considerably reduced. In addition, the hole mobility values of the layers were investigated using SCLC results, as reported in ref. 37, 40 and 41. The hole mobility (μ_h) of the perovskite layer after the addition of Pyr IL was increased to 1.25×10^{-4} cm^2 V^{-1} s^{-1} compared to 2.28×10^{-5} cm^2 V^{-1} s^{-1} for the control sample.

These enhancements could reduce carrier recombination and are supposed to boost the FF and V_{OC} of the device.

The presence of Pyr-IL not only enhances the PCE but also contributes to the overall stability and performance of FSCs. Fig. 7 illustrates the normalized efficiency of Pyr-mediated FSCs and control devices over time under different conditions. Specifically, Fig. 7a demonstrates the ambient air stability of unsealed FSCs at room temperature in dark conditions. The graph clearly shows that the Pyr-mediated FSCs exhibit higher stability compared to the control FSCs, as their efficiency declines at a slower rate over time. It is important to investigate the effect of introducing Pyr-IL on the stability of the device under continuous illumination, considering the stability of the perovskite material itself and the interfacial stability of FSC (Fig. 7b). After 72 days of continuous illumination, the unsealed Pyr-mediated FSCs maintained 80% of their initial efficiency, while the unsealed control devices quickly lost their initial efficiency. This improvement in stability can be attributed to the introduction of Pyr-IL, which helps passivate interface defects and suppress ion migration. Consequently, the Pyr-IL modification significantly enhances the stability of the FSCs compared to the control devices.

Table 2 lists the PCEs and HI values of different reported sequential-deposited PSCs and compares them with those of the current study. The 21.72% efficiency obtained here with the

Table 2 Summary of perovskite solar cells fabricated based on sequential deposition method and their efficiencies and hysteresis indexes

Perovskite material	Strategy	PCE (%)	Hysteresis index (%)	Ref.
	Perovskite seeds added to PbI$_2$ layer	21.50	1.86	42
FAPbI$_3$	Biguanide hydrochloride added to PbI$_2$ layer	22.12	Almost eliminated	43
FAPbI$_3$	Added 4-(trifluoromethyl)benzylammonium iodide to perovskite	22.40	1.83	44
FAPbI$_3$	Temperature-assisted crystal growth	18.41	Not reported	45
FAPbI$_3$	Cesium acetate added to PbI$_2$ layer	22.19	Not reported	46
(MAFA)Pb(IBr)$_3$	Methylammonium thiocyanate added to PbI$_2$ layer	20.40	Not reported	47
Cs$_{0.2}$MA$_{0.2}$FA$_{0.6}$Pb(I$_{0.22}$Br$_{0.78}$)$_3$	FABr, PbBr$_2$, and MABr added to PbI$_2$ layer	21.50	4.88	48
(MAFA)Pb(IBr)$_3$	Introduced δ-CsPbI$_2$Br into PbI$_2$ layer	21.62	7.17	49
FAPbI$_3$	Added pyrrolidinium to PbI$_2$ layer	21.72	3.44%	This study

assistance of Pyr-based modification is comparable with reported PCE values in literature.

4. Conclusions

This work demonstrates the significant benefits of incorporating pyrrolidinium (Pyr) ionic liquid into the PbI_2 layer of FSCs. The incorporation of Pyr-ionic liquid into the PbI_2 layer of FPSCs has shown encouraging results in improving the overall performance and stability of the fabricated devices. The addition of Pyr was found to substantially improve the PCEs of the devices, with the highest PCE of 21.72% achieved with a 1.75 wt% Pyr concentration. The experimental results showed that the optimal concentration of Pyr-IL in the perovskite layer can lead to enhanced conversion efficiency, enhanced charge carrier dynamics, and better growth of crystal within the perovskite film. This led to reduced defect density, reduced recombination, and suppressed charge transfer resistance at the interfaces. Furthermore, the Pyr-IL modification was shown to improve the stability of FSCs under ambient air and continuous illumination conditions, further emphasizing its potential for practical applications in renewable and clean energy resources. These results highlight the significant impact of Pyr-IL in advancing the performance and stability of FSCs, showing the way for upcoming research and development in the field of solar energy technologies.

Data and code availability

The data that support the findings of this study are available from the corresponding author upon reasonable request.

Author contributions

All authors contributed equally in this paper.

Conflicts of interest

The authors declare that they have no conflict of interest.

Acknowledgements

References

1 Q. Wang, N. Phung, D. Di Girolamo, P. Vivo and A. Abate, Enhancement in lifespan of halide perovskite solar cells, *Energy Environ. Sci.*, 2019, **12**(3), 865–886.

2 D. Zhou, T. Zhou, Y. Tian, X. Zhu and Y. Tu, Perovskite-based solar cells: materials, methods, and future perspectives, *J. Nanomater.*, 2018, **2018**, 1–15.

3 M. Dehghanipour, A. Behjat, A. Shabani and M. Haddad, Toward desirable 2D/3D hybrid perovskite films for solar cell application with additive engineering approach, *J. Mater. Sci.: Mater. Electron.*, 2022, **33**(16), 12953–12964.

4 L. Qiu, L. K. Ono and Y. Qi, Advances and challenges to the commercialization of organic–inorganic halide perovskite solar cell technology, *Mater. Today Energy*, 2018, **7**, 169–189.

5 A. Kojima, K. Teshima, Y. Shirai and T. Miyasaka, Organometal halide perovskites as visible-light sensitizers for photovoltaic cells, *J. Am. Chem. Soc.*, 2009, **131**(17), 6050–6051.

6 D. A. Noori, A. Behjat and M. Dehghanipour, Operational stability study of hole transport-free perovskite solar cells using lithium fluoride in electron transport layer, *J. Mater. Sci.: Mater. Electron.*, 2023, **34**(7), 592.

7 J. J. Yoo, G. Seo, M. R. Chua, T. G. Park, Y. Lu, F. Rotermund, *et al.*, Efficient perovskite solar cells via improved carrier management, *Nature*, 2021, **590**(7847), 587–593.

8 H. Chen, C. Liu, J. Xu, A. Maxwell, W. Zhou, Y. Yang, *et al.*, Improved charge extraction in inverted perovskite solar cells with dual-site-binding ligands, *Science*, 2024, **384**(6692), 189–193.

9 Y. Ma, Y. Zhang, M. Liu, T. Han, Y. Wang and X. Wang, Improving the performance of quantum dot sensitized solar cells by employing Zn doped CuInS 2 quantum dots, *Adv. Compos. Hybrid Mater.*, 2022, 1–8.

10 V. Murugadoss, D. Y. Kang, W. J. Lee, I. G. Jang and T. Geun Kim, Fluorine-induced surface modification to obtain stable and low energy loss zinc oxide/perovskite interface for photovoltaic application, *Adv. Compos. Hybrid Mater.*, 2022, **5**(2), 1385–1395.

11 B. He, Y. Xu, J. Zhu and X. Zhang, Effects of the doping density of charge-transporting layers on regular and inverted perovskite solar cells: numerical simulations, *Adv. Compos. Hybrid Mater.*, 2021, **4**, 1146–1154.

12 J. Jeong, M. Kim, J. Seo, H. Lu, P. Ahlawat, A. Mishra, *et al.*, Pseudo-halide anion engineering for α-FAPbI3 perovskite solar cells, *Nature*, 2021, **592**(7854), 381–385.

13 M. K. Mohammed, M. I. Abualsayed, A. M. Alshehri, A. Kumar, M. Dehghanipour, A. R. Sh, *et al.*, Synergistic Effects of Energy Level Alignment and Trap Passivation via 3, 4-Dihydroxyphenethylamine Hydrochloride for Efficient and Air-Stable Perovskite Solar Cells, *ACS Appl. Energy Mater.*, 2024, **7**(3), 1358–1368.

14 J. W. Lee, D. J. Seol, A. N. Cho and N. G. Park, High-efficiency perovskite solar cells based on the black polymorph of HC (NH2) 2PbI3, *Adv. Mater.*, 2014, **26**(29), 4991–4998.

15 C. Ma and N.-G. Park, Paradoxical approach with a hydrophilic passivation layer for moisture-stable, 23% efficient perovskite solar cells, *ACS Energy Lett.*, 2020, **5**(10), 3268–3275.

16 M. Dehghanipour, A. Behjat and H. A. Bioki, Fabrication of stable and efficient 2D/3D perovskite solar cells through post-treatment with TBABF 4, *J. Mater. Chem. C*, 2021, **9**(3), 957–966.

17 H. Yu, H. Lu, F. Xie, S. Zhou and N. Zhao, Native defect-induced hysteresis behavior in organolead iodide perovskite solar cells, *Adv. Funct. Mater.*, 2016, **26**(9), 1411–1419.

18 M. L. Agiorgousis, Y.-Y. Sun, H. Zeng and S. Zhang, Strong covalency-induced recombination centers in perovskite solar cell material CH3NH3PbI3, *J. Am. Chem. Soc.*, 2014, **136**(41), 14570–14575.

19 Q. Wang, B. Chen, Y. Liu, Y. Deng, Y. Bai, Q. Dong, *et al.*, Scaling behavior of moisture-induced grain degradation in polycrystalline hybrid perovskite thin films, *Energy Environ. Sci.*, 2017, **10**(2), 516–522.

20 J. P. Hallett and T. Welton, Room-temperature ionic liquids: solvents for synthesis and catalysis. 2, *Chem. Rev.*, 2011, **111**(5), 3508–3576.

21 M. Smiglak, J. M. Pringle, X. Lu, L. Han, S. Zhang, H. Gao, *et al.*, Ionic liquids for energy, materials, and medicine, *Chem. Commun.*, 2014, **50**(66), 9228–9250.

22 S. Ghosh and T. Singh, Role of ionic liquids in organic-inorganic metal halide perovskite solar cells efficiency and stability, *Nano Energy*, 2019, **63**, 103828.

23 X. Deng, L. Xie, S. Wang, C. Li, A. Wang, Y. Yuan, *et al.*, Ionic liquids engineering for high-efficiency and stable perovskite solar cells, *Chem. Eng. J.*, 2020, **398**, 125594.

24 D. T. Moore, H. Sai, K. W. Tan, D.-M. Smilgies, W. Zhang, H. J. Snaith, *et al.*, Crystallization kinetics of organic–inorganic trihalide perovskites and the role of the lead anion in crystal growth, *J. Am. Chem. Soc.*, 2015, **137**(6), 2350–2358.

25 M. Shahiduzzaman, K. Yamamoto, Y. Furumoto, T. Kuwabara, K. Takahashi and T. Taima, Ionic liquid-assisted growth of methylammonium lead iodide spherical nanoparticles by a simple spin-coating method and photovoltaic properties of perovskite solar cells, *RSC Adv.*, 2015, **5**(95), 77495–77500.

26 Y. Wan, S. Dong, Y. Wang, L. Yang, W. Qin, H. Cao, *et al.*, Ionic liquid-assisted perovskite crystal film growth for high performance planar heterojunction perovskite solar cells, *RSC Adv.*, 2016, **6**(100), 97848–97852.

27 J. Seo, T. Matsui, J.-P. Correa-Baena, F. Giordano, M. Saliba, *et al.*, Ionic liquid control crystal growth to enhance planar perovskite solar cells efficiency, *Adv. Energy Mater.*, 2016, **6**(20), 1600767.

28 W. Wu, Y. Li, A. Abate and M. Wei, 2-Methylimidazole as an interlayer for the enhancement of the open-circuit voltage in perovskite solar cells, *J. Power Sources*, 2020, **450**, 227714.

29 N. Zhou, Y. Shen, Y. Zhang, Z. Xu, G. Zheng, L. Li, *et al.*, CsI Pre-Intercalation in the Inorganic Framework for Efficient and Stable FA1−x CsxPbI3 (Cl) Perovskite Solar Cells, *Small*, 2017, **13**(23), 1700484.

30 G. Murugadoss, R. Thangamuthu and M. R. Kumar, Formamidinium lead iodide perovskite: Structure, shape and optical tuning via hydrothermal method, *Mater. Lett.*, 2018, **231**, 16–19.

31 A. M. Naji, S. H. Kareem, A. H. Faris and M. K. Mohammed, Polyaniline polymer-modified ZnO electron transport material for high-performance planar perovskite solar cells, *Ceram. Int.*, 2021, **47**(23), 33390–33397.

32 D. Shi, V. Adinolfi, R. Comin, M. Yuan, E. Alarousu, A. Buin, *et al.*, Low trap-state density and long carrier diffusion in organolead trihalide perovskite single crystals, *Science*, 2015, **347**(6221), 519–522.

33 N.-G. Park, Crystal growth engineering for high efficiency perovskite solar cells, *CrystEngComm*, 2016, **18**(32), 5977–5985.

34 M. Long, T. Zhang, W. Xu, X. Zeng, F. Xie, Q. Li, *et al.*, Large-grain formamidinium PbI3–xBrx for high-performance perovskite solar cells via intermediate halide exchange, *Adv. Energy Mater.*, 2017, **7**(12), 1601882.

35 M. Li, J. Zhou, L. Tan, H. Li, Y. Liu, C. Jiang, *et al.*, Multifunctional succinate additive for flexible perovskite solar cells with more than 23% power-conversion efficiency, *Innovation*, 2022, **3**(6), 100310.

36 D. Dastan, M. K. Mohammed, R. Sh Alnayli, M. S. Majeed, D. S. Ahmed, A. K. Al-Mousoi, *et al.*, Achieving Well-Oriented FAPbI3 Perovskite Photovoltaics by Cyclohexane Modification, *Langmuir*, 2024, **40**(14), 7560–7568.

37 S. H. Kareem, M. H. Elewi, A. M. Naji, D. S. Ahmed and M. K. Mohammed, Efficient and stable pure α-phase FAPbI3 perovskite solar cells with a dual engineering strategy: additive and dimensional engineering approaches, *Chem. Eng. J.*, 2022, **443**, 136469.

38 H. Zhou, W. Wang, Y. Duan, R. Sun, Y. Li, Z. Xie, *et al.*, Glycol Monomethyl Ether-Substituted Carbazolyl Hole-Transporting Material for Stable Inverted Perovskite Solar Cells with Efficiency of 25.52%, *Angew. Chem., Int. Ed.*, 2024, **63**(33), e202403068.

39 P. Zhao, D. He, S. Li, H. Cui, Y. Yang, W. Chen, *et al.*, Design of a Unique Hole-Transporting Molecule via Introducing a Chloro-Involved Chelating Moiety for High-Performance Inverted Perovskite Solar Cells, *Adv. Funct. Mater.*, 2024, **34**(4), 2308795.

40 T. Yeşil, A. Mutlu, S. Siyahjani Gültekin, Z. G. Günel and C. Zafer, Enhanced Hole Mobility of p-Type Materials by Molecular Engineering for Efficient Perovskite Solar Cells, *ACS Omega*, 2023, **8**(30), 27784–27793.

41 Q. Fu, H. Liu, Y. Gao, X. Cao, Y. Li, Y. Yang, *et al.*, Tunable molecular packing of dopant-free hole-transport polymers for perovskite solar cells, *ACS Energy Lett.*, 2023, **8**(7), 2878–2885.

42 Y. Zhao, H. Tan, H. Yuan, Z. Yang, J. Z. Fan, J. Kim, *et al.*, Perovskite seeding growth of formamidinium-lead-iodide-based perovskites for efficient and stable solar cells, *Nat. Commun.*, 2018, **9**(1), 1607.

43 X. Ma, P. Chen, J. Luo, N. Yang, D. Luo, R. Su, *et al.*, Perovskite Seeding Approach of Two-Step Sequential Deposition for Efficient Solar Cells, *ACS Appl. Energy Mater.*, 2024, **7**(10), 4540–4548.

44 H. B. Lee, N. Kumar, S. Cho, S. Hong, H. H. Lee, H. J. Kim, *et al.*, Intercalation of Ammonium Cationic Ligands Enabled Grain Surface Passivation in Sequential-Deposited Perovskite Solar Cells, *Adv. Energy Sustainability Res.*, 2023, **4**(1), 2200128.

45 W. He, J. Hu, C. Chen, Y. Chen, L. Zeng, X. Zhang, *et al.*, Temperature-assisted crystal growth of photovoltaic α-phase FAPbI3 thin films by sequential blade coating, *ACS Appl. Mater. Interfaces*, 2020, **12**(50), 55830–55837.

46 B. J. Kim and G. Boschloo, Beneficial effects of cesium acetate in the sequential deposition method for perovskite solar cells, *Nanoscale*, 2021, **13**(26), 11478–11487.

47 D. Li, T. Xia, W. Liu, G. Zheng, N. Tian, D. Yao, *et al.*, Methylammonium thiocyanate seeds assisted heterogeneous nucleation for achieving high-performance perovskite solar cells, *Appl. Surf. Sci.*, 2022, **592**, 153206.

48 Q. Li, Y. Zhao, W. Zhou, Z. Han, R. Fu, F. Lin, *et al.*, Halogen engineering for operationally stable perovskite solar cells via sequential deposition, *Adv. Energy Mater.*, 2019, **9**(46), 1902239.

49 F. Qiu, J. Sun, Z. Zhang, T. Shen, H. Liu and J. Qi, Achieving stable and high-efficiency (> 21%) lead halide perovskite solar cells with δ-CsPbI2Br seed–assisted growth strategy, *Mater. Today Energy*, 2021, **21**, 100837.